Hydrologic Implications of Dynamically Downscaled Climate Projections in the Southwestern United States

Matthew B. Switanek, Peter A. Troch, Christopher L. Castro, Hsin-I Chang, Thang Luong, Matej Durcik and Eleonora Demaria

1. Introduction

Climate change in the 21st century is expected to substantially impact regional water supplies across the world. The population and agricultural centers in the southwestern United States are particularly susceptible to changes in streamflow quantity. This is due to this region's lack of abundant surface water reserves and a dwindling supply of groundwater. The Colorado River Basin and the headwaters of the Rio Grande River are the lifelines of the Southwest region. These rivers are heavily regulated and, as a result, any reductions in these streamflows would severely impact the region's economic and environmental health. Therefore, it is essential to understand how climate change could affect future water resources in river basins such as the Colorado and Rio Grande.

The General Circulation Models (GCMs) used in the IPCC (Intergovernmental Panel on Climate Change), on average, project that global mean surface temperatures are going to rise [*Barnett et al.*, 2005; *Christensen et al.*, 2004; *Held and Soden*, 2006; *Kharin and Zwiers*, 2000, 2005]. More specifically to the Southwest region, the GCMs have a consensus on the direction of temperature trends (increasing), while they are less certain about what changes can be expected to precipitation at the mid-latitudes. GCMs are invaluable in providing general forecasts of future climate, though they are too course (typically 150-300 km) to provide the detail that is necessary to accurately assess regional dynamics [*Castro et al.*, 2005*; Maurer and Hidalgo*, 2008; *Woods et al.*, 2004*; Von Storch et al*., 1993]. Ideally, in an effort to understand the role that climate change plays in a particular region such as the Southwest, one would downscale GCM forecasts with a Regional Climate Model (RCM) that produce

variables that preserve a level of spatial coherence and physical plausibility. This physical plausibility of the RCMs allows for non-stationarity in future realizations of the climate variables [*Milly*, 2010]. Until recently, dynamically downscaling multi-decade simulations of General Circulation Models (GCMs) were not reasonable for environmental impact studies of relatively large regions [*Maurer et al.*, 2008; *Sungwook et al*., 2012]. This was due to the amount of time and resources required to run an RCM for many decades. Past climate change studies have typically statistically downscaled GCMs. Statistical downscaling is efficient and provides an important glimpse into potential environmental impacts the future contains. Importantly, however, statistical downscaling cannot account for non-stationarity. While the methodology can incorporate trends to the data, any extreme events or systematic changes to a climate variable's variance cannot be reasonably implemented [*Dominguez et al.*, 2012]. Additionally, any nonlinearities inherent to the physical system might not be corrected applied to climate variables relying on statistics alone.

These changes to the climate subsequently lead to earlier timing of snowmelt [*Barnett et al.*, 2005; *Cayan*, 2000; *Stewart et al.*, 2004]. Additional studies have pointed out that the streamflow distributions may not only be shifting, but also may be decreasing/increasing in volume as well [*Christensen et al.*, 2004; Allen et al., 2002; *Acharya et al.*, 2012]. *Goa et al.* [2011] used RCMs to dynamically downscale three GCMs and found two projected a 16% decrease in streamflow, while one projected a 5% increase. These values were calculated as relative changes between the periods 2040-2069 and 1970-1999. Our study also uses an RCM to dynamically downscale two GCMs, but we bias correct the RCM climate variables before forcing the hydrologic model. Additionally, we look at relative changes over a longer period of projected time (~70 years). Finally, we investigate the hydrologic response at selected subbasins in the Colorado river and also add the headwaters of the Rio Grande river.

Allen and Ingram [2002] write, "In the absence of objective probabilistic forecasts with numerical models that systematically investigate the range of possible responses of the hydrologic

cycle to anthropogenic climate change, we have here attempted to constrain the expected changes by other means." Ideally, one would like to dynamically downscale many of the GCMs used in the IPCC report under a range of different climate scenarios. With the continued expansion of computational resources, this will soon be possible. Before dynamically downscaling multiple decades of GCMs becomes the new norm, the authors attempt to provide an first glimpse into the climatic and hydrologic changes that are part of the distribution of future realizations. We have chosen two GCMs that have historically performed well in simulating the climate over the southwestern United States. This study used two dynamically downscaled GCMs for the region encompassing the southwestern United States and northwestern Mexico. The two GCM climate models used were the HadCM3 and the MPI-ECHAM5. They were downscaled with the Weather and Research Forecasting (WRF) regional scale climate model. This study sets out to investigate whether the overall quantity of streamflow is projected to change in selected subbasins of the Colorado and Rio Grande rivers.

2. Data and Methodology

2.1 Study Locations and Data

The Salt and Verde basins and Rio Grande headwaters are shown in Figure 1. USGS streamflow gauges 09498500, 09508500, and 08220000 are used as the hydrologic outflow points for the Salt, Verde, and Rio Grande, respectively. The Salt and Verde basins have areas of 11,100 km^2 and 15,200 km^2 above the streamflow gauges, while the Rio Grande headwaters has an area of 3,400 km^2. Average streamflows of $2.09*10^6$ m^3/day, $2.03*10^6$ m^3/day, and $1.43*10^6$ m^3/day are seen at the Salt, Verde and Rio Grande gauges, respectively.

The Weather and Research Forecasting (WRF) model has been used extensively as a regional-scale atmospheric model. Data from two General Circulation Models (GCMs) from IPCC Fourth Assesment Report, that have historically performed well over the Southwest, were chosen to force the

WRF model. These models are the HadCM3 and the MPI-ECHAM5 (MPI from here on). WRF dynamically downscales climate data from these two GCMs under the A1B (medium emission scenario or 'Business as Usual', CO2 concentration 700ppm by 2100) scenario at a resolution of 32 km. Additionally, an atmospheric reanalysis data set (NCEP-NCAR) was used to provide a measure of how well the WRF model can simulate regional-scale weather events that comprise the climate. Later in the paper, any time we refer to the HadCM3, MPI, and NCAR, we are more specifically referring to the dynamically-downscaled climate data from these GCMs.

The hydrologic modeling is performed using the Variable Infiltration Capacity (VIC) model. The VIC model represents surface and subsurface hydrologic processes on spatially distributed grid cells. Distinguishing characeristics of the model include the representation of subgrid scale variability in vegetation coverage, topography, precipitation, and soil moisture storage capacity. The subsurface is represented by three soil layers. Evapotranspiration can occur from soil moisture in the three layers, while slow repsonse runoff or baseflow is only generated from the third layer. To represent the sub-grid spatial variability in soil moisture storage, the model assumes that the infiltration capacity is a non-linear function of the soil moisture storage within the gridcell. Simulations in this study were performed at a daily time step with a 12.5 km resolution (1/8 degree).

2.2 Model Calibration and Bias Correction

2.2.1 VIC Model Calibration

Calibration of the VIC model was performed using Ed Maurer's climate data set as observed data [*Maurer et al.*, 2002]. VIC was calibrated on daily streamflow values using the Shuffled Complex Evolution algorithm. The Kling-Gupta efficiency (KGE) parameter [*Gupta et al.*, 2009] was used as the objective measure of skill between modeled and observed streamflows. The KGE is defined as

$$KGE = 1 - sqrt((1-a)^2 + (1-b)^2 + (1-r)^2), \quad (1)$$

where a is the ratio of the means, b is the ratio of the coefficient of variations, and r is the correlation

coefficient. The KGE skill measure provides the optimum parameter set that has the least Euclidian distance between simulations and observations. Typically, the measure will make sacrifices in correlation, with respect to another skill measure such as the Nash-Sutcliffe efficiency parameter, but makes substantial improvements in bias and variance explained. During the calibration process, it became apparent that no amount of model calibration could reduce a substantial amount of positive bias (see Figure 2). The model was always predicting, on average, more streamflow. Given the methods of sampling streamflow versus precipitation, at the basin scale, we see streamflow data as being more certain than interpolated precipitation data. Therefore, in order to have the model perform better, we adjusted the precipitation data by a constant multiplier. This constant multiplier of precipitation was then an additional parameter in the model calibration. Figure 2 illustrates the effectiveness of the calibration procedure. The Salt and Rio Grande clearly show the amount of positive bias in the streamflow forecasts prior to calibration. Each component of the KGE was improved in the calibration process, except for the Rio Grande's correlation, which slightly decreased (a trade-off to drastically improve the bias and variance explained).

2.2.2 Bias Correction of Climate Data

Bias correction of precipitation, temperature and wind were all performed independently. Bias corrections of precipitation, temperature and wind were all performed with a modified form of distribution mapping [*Teutschbein and Seibert*, 2012; *Wood et al.*, 2004]. We use a distributional mapping method with fitted gamma distributions for precipitation, and normal distributions for the other variables. The bias correction of precipitation had to meet a number of criteria. First, the distributions of the simulated and observed precipitation had to closely match for each subset time of the year. Second, the frequency of rain events had to match. Third, changes in the distributions and frequencies of precipitation events, at different seasons, had to be preserved.

To begin with, precipitation data was bias corrected on a 21-day moving window (precipitation,

maximum temperature, minimum temperature, and wind all use a 21-day moving window to compute the bias corrected data for a particular day). Consider the bias correction of the precipitation values of HadCM3 and MPI data for all years that overlap with observations (1968-2010 and 1950-2010, respectively) for the date January 11. Positive precipitation values between January 1st and January 21st for these years were used to fit the gamma distribution parameters a and b for the observed and simulated data. For each value of precipitation (x-axis on the fitted gamma cumulative distribution function (CDF)) that occurred on January 11th, its corresponding cumulative distribution is found (y-axis on the same CDF). The same cumulative distribution is then located on the fitted gamma distribution of the observations for the same day. And finally, the bias corrected precipitation would be the corresponding value on the x-axis. Next, we need to account for the difference between the amount of rain days for the observations and the projected climate. The climate models were always forecasting more rain days. Therefore, we randomly removed precipitation events to match the percentage of rain days, seen in the observed period, for each 21-day moving window.

The next step was to bias correct the future time period of precipitation. First, the percentage differences between the mean and standard deviations were used to shift the observed gamma distribution. With a two parameter gamma distribution, the mean and the variance are defined as $\alpha*\beta$ and $\alpha*\beta^2$, respectively. Therefore, it is clear that for a gamma distribution β = variance/mean and α = mean/β. We find the mean and the variance of both the gamma distributions in the time overlapping the observations (overlapping time period referred to as OLTP, 1968-2010 for HadCM3 and 1950-2010 for MPI) and the projected time periods (projected time period referred to as PJTP, 2011-2079 for HadCM3 and 2011-2080 for MPI). The ratio by which the mean and the variance of the PJTP differs with respect to the OLTP is then multiplied by the mean and variances of the observed distribution. We then can use these new mean and variance values to solve for the α and β of a new gamma distribution. This gamma distribution will then have the same proportional shift, with reference to the observational distribution, as the shift between projected and past precipitation. The first two steps of the bias

correction, outlined in this paragraph, are then repeated using the shifted observed gamma distribution to bias correct future precipitation values.

The well established bias-correction and spatial downscaling (BCSD) methodology [Wood et al., 2004] is different than what is presented here in the following ways. Empirical distributions are used for BCSD while, we map to any location on a fitted gamma distribution. Second, we match the closest whole number of days of rain about our moving window. If one starts with a model with more rain days, this appears to be preserved in BCSD, though each value is scaled so that the monthly means match up. Because streamflow can respond differently to the same precipitation amount spread over a varied number of days, we attempt to preserve the observed frequency of rain events.

The bias correction of maximum and minimum temperature were also performed using a 21-day moving window. In bias correcting the temperatures, the means and variances of the OLTP for the HadCM3 and MPI models are shifted to match those of observations. However, the trends seen in the models are preserved. This is so that the models' physical representations of a potential future climate is not constrained by the trends that we have observed in the past. Future trends can be different than what the past suggests. Lastly, and similarly to precipitation, differences in the distributions and the trends between the OLTP and the PJTP were preserved.

Often a trend was seen in both the observed and simulated temperatures (e.g., moving through the years for a specific day). This trending inflates the variance. This is due to the fact that the differences between the values in a time series and a fixed mean is greater than the differences between the values and their accompanying trend line (provided that there is a non-zero trend). Therefore, the standard deviation of temperature for a particular day's window is

$$Tstd = sqrt((T - Treg)^2 / (n-1)) \quad (2)$$

where T is the temperature time series for a specific day, Treg is the regression line of the temperature time series, and n is the number of values in T. The bias correction of maximum and minimum temperature values in the OLTP was calculated as

$$T_{bc} = T_{mod} + T_{trnd\_mov} - T_{trnd\_ind}$$

(3)

where Tbc is bias corrected temperature and

$$T_{mod} = T_{obs\_mean} + (T_{gcm} - T_{gcm\_mean}) * (T_{obs\_std}/T_{gcm\_std})$$

(4)

and

$$T_{trnd\_mov} = T_{gcm\_trnd\_mov} + (T_{obs\_mean} - T_{gcm\_mean})$$

(5)

and Ttrnd_ind is the regression line of Tmod. Tbc is the bias corrected maximum or minimum temperature. Tmod is the modified temperature data where Tobs_mean, Tgcm_mean, Tobs_std, and Tgcm_std are means and standard deviations of the observations and the OLTP GCM (HadCM3 or MPI) values within the moving window, respectively. Ttrnd_mov is the adjusted 21-day moving window trend, where Tgcm_trnd_mov is the moving window trend of the raw HadCM3 or MPI data. This provides a trend line of the OLTP GCM data with its mean identical that of Tobs_mean. Hence, the OLTP Tbc is found by first calculating the two time series of Tmod and Ttrnd_mov. Second, the regression line of Tmod is obtained. Lastly, the bias corrected temperature, Tbc, will be Tmod plus the moving window trend (Ttrnd_mov) minus the time series of the individual day's trend (Ttrnd_ind). Calculating Tmod does the work of the bias correction and shifts the mean and variance of the OLTP GCM temperatures to match those of observations. The act of adding Ttrnd_mov and subtracting Ttrnnd_ind effectively is shifting the individual day's temperature trend to match that of the moving window trend.

Bias correcting temperature in the projected time period is very similar with a couple of small modifications. Equation 4 now becomes

$$T_{mod} = T_{obs\_mean} + (T_{gcm2} - T_{gcm\_mean2}) * (T_{obs\_std}/T_{gcm\_std2}) \quad * (T_{gcm\_std2}/T_{gcm\_std1})$$

(6)

where the subscripts 1 and 2 represent the overlapping and projected time periods, respectively. The additional term in equation 6, with respect to equation 4, increases or decreases the variance proportionally to the ratio of the standard deviations seen in the projected and overlapping time periods. Equation 6 reduces to

$$T_{mod} = T_{obs\_mean} + (T_{gcm2} - T_{gcm\_mean2}) * (T_{obs\_std}/T_{gcm\_std1}) \quad (7)$$

Lastly, equation 5 is now

$$T_{trnd\_mov} = T_{gcm\_trnd\_mov2} + (T_{obs\_mean1} - T_{gcm\_mean1}) \quad (8)$$

where the trend line of the projected time period is further offset by the difference between the observed and OLTP temperatures.

Wind was bias corrected using equations 6 and 9, with wind in place of temperature, for the overlapping and projected time periods, respectively. The modified wind is the bias corrected wind because no statistically significant trending of wind was discernible, and therefore no trend adjustments were implemented.

3. Results

3.1 Calibration and Bias Correction

The results of the VIC model calibration are apparent in Figure 2. Prior to model calibration, the Salt, Verde and Rio Grande basins had KGE values of -.73, .17, and -.44, respectively (these values correspond to the subplots in the upper row of Figure 2). After model calibration, the Salt, Verde and Rio Grande had KGE values of .57, .65 and .77, respectively (lower row of subplots in Figure 2). In order to observe how well the WRF model is simulating weather events that make up the longer-term climate, WRF was forced with the NCEP-NCAR Final Analyses data set which has a resolution of 1x1 degree grids. Using the resulting dynamically downscaled NCEP-NCAR-WRF data to force VIC (at

1/8x1/8 degree grids) for the years 1979-2000, we obtain KGEs of .55, .64, and .74 for the Salt, Verde and Rio Grande, respectively. Therefore, WRF is doing well in reproducing weather events and their timing.

Figure 3 shows examples of the effectiveness of the bias correction. Figure 3a shows the cumulative gamma distribution of the raw, dynamically-downscaled HadCM3 OLTP data (for January 31st) in green while the observed distribution is the black dashed line. After bias correcting the precipitation, we have the distribution shown by the blue line. The bias corrected distribution is seen to be very similar to the observed distribution. Figure 3b illustrates, for temperature, how we have treated the OLTP and the PJTP differently. Again the green line is the raw HadCM3 data (for January 13th). The figure shows how means are shifted up and the trends are preserved in each period. In this particular case, the variance was only slightly increased in the OLTP to match observations.

The resulting distributional changes before and after bias correction are shown in Figure 4. The upper three rows show the α parameter for the precipitation distributions and the mean for the distributions corresponding to maximum temperature, minimum temperature and wind. The lower three rows show the β parameter for the precipitation distributions and the standard deviation for the distributions corresponding to the other climate variables. The x-axis is the sorted elevation values in the Salt river basin. The y-axis is the days of the year with the beginnings of each month being labeled. The first and fourth rows show the α or mean values and the β or standard deviation values, respectively, prior to bias correction of the HadCM3 model. The second and fifth rows show the same distributional values but for the observed data. The third and sixth rows show the distributional values after bias correcting the HadCM3 climate data. In essence, we want the climatological distributions of each gridcell in the Salt river basin (x-axis), throughout the year (y-axis) to as closely match observations as possible. This means that it is desirable to have the second and third rows for each column to be relatively indistinguishable from one another. Similarly, rows five and six should look very similar. As an example, it can be seen that prior to bias correction the mean minimum temperature

(subplot is row one, column three) was too high especially at higher elevations in the warmer months (top of subplot for months of June, July, August and September). In August at high elevations, the HadCM3 model had a mean minimum temperature near 15°C, while the observations had a mean minimum temperature near 6°C. During the same time of year and at the same elevations in the Salt, the standard deviation of the minimum temperature is being underestimated. In August at high elevations, the HadCM3 model had a standard deviation for the minimum temperature near 1°C, while the observations had a standard deviation near 2°C. It can clearly be seen how closely rows two and three, as well as five and six, resemble each other. Visually, after bias correction the climatological distributions of the HadCM3 model are very close to the observed distributions. How much improvement in quantitatively representing the climatology can be seen by bias correcting the climate data?

Mean absolute error was used to quantify the improvement in matching the observed distributions in the OLTP due to bias correction. The mean absolute error (MAE) is the average of the absolute difference between each value in the sorted empirical distributions (using the 21-day moving windows). Smaller MAE values indicate that the observed and simulated distributions are closer to one another than with larger MAE values. MAE is an open ended scale above zero, so we would like to see a substantial improvement in the reduction of MAE values due to bias correction. Figure 5 shows the change in MAE before and after the bias correction. The left column shows the MAE values between the raw HadCM3 and observed data. Similarly to Figure 4, the x-axis is the sorted elevation values in the Salt river basin, while the y-axis is the days of the year with the beginnings of each month being labeled. The colorbar is logarithmic values of MAE. Figure 5 illustrates substantial reductions in the MAE as a result of bias correcting the HadCM3 model for the Salt river basin. Table 1 provides the spatial (y-axis of Figure 5) and temporal (x-axis of Figure 5) averages of the MAE values for each climate variable using both models for the three basins. For example, the average MAE for the top left subplot (raw precipitation) in Figure 5 is 1.95mm. After bias correction, the MAE is reduced to .38mm.

Overall, the precipitation MAE is reduced, on average, across the three basins for the two models by 84%. The maximum temperature, minimum temperature, and wind MAE values were reduced by 92%, 94% and 96%, respectively.

3.2 Projected Climate Change

Now that the bias corrected HadCM3 and MPI models are more accurately simulating the seasonal climate patterns and distributions, how is the climate in these basins expected to change in the future due to the A1B ("Business as Usual") climate change scenario? The upper row of Figure 6 shows the the percentage change in average precipitation in the PJTP with respect to the OLTP. The x and y-axes are again the same as in Figures 4 and 5. The bottom two rows of Figure 6 are the differences in average maximum and minimum temperature, respectively. The HadCM3 model is projecting more precipitation in the January and June months for the time period 2011-2079 with respect to the period 1968-2010. While late April and November months are projected to be drier. The MPI model is, on average projecting a future with less precipitation (for the time period 2011-2080 with respect to the period 1950-2010). Both models are projecting, on average, between a 1°C and 3°C increase in temperature. Changes in wind in the future time period were negligible with respect to the past period. How do these changes in precipitation and temperature translate to differences in anticipated future water availability?

3.3 Projected Hydrologic Change

Figure 7 illustrates how the probability of exceedance plots change for streamflow between the PJTP and the OLTP. The blue lines show how each projected future streamflow value (expressed as a probability of exceedance on the x-axis) changes with respect to historical flows (y-axis is percentage change). The black, dotted lines are the average percentage changes in overall streamflow. For example, forcing the VIC model with HadCM3 in the Salt, approximately a 15% decrease in

streamflow at high values is projected for future flows with respect to what has historically been observed. Projected future climate, with both the HadCM3 and MPI models, show decreased streamflow at all values for all three basins except a slight increase at low flows in the Verde (where VIC is forced by HadCM3). The HadCM3 model is projecting on average a 15%, 20% and 22% decrease in future streamflow for the Salt, Rio Grande and Verde, respectively. The MPI model is projecting on average a 36%, 31% and 38% decrease in future streamflow for the Salt, Rio Grande and Verde, respectively. Performing a t-test for all six instances (both models for the three basins), the PJTP streamflow means were found to be statistically significantly different ($p < .01$) than the OLTP means.

Changes in snow water equivalent (SWE) and baseflow appear to explain these projected changes to streamflow in the three basins. Figure 8 shows critical components to the water budget as simulated by VIC for the Salt. Spatially and temporally averaging evaporation and surface runoff for HadCM3, there is no clear direction of change for the PJTP with respect to the OLTP. While for MPI, there is less surface runoff but also less evaporation. It can clearly be seen that the substantial percentage decreases in SWE and baseflow are dominating the decreases that are being projected in overall streamflow.

3. Discussion and Conclusions

This study set out to observe if climate projections in the Southwest, under the A1B scenario, would have any discernible affects on the hydrology. With the state of the science, we found that there is indeed a noticeable affect. As a first step, we found that both GCMs, after downscaling, consistently projected future temperatures to increase between a 1°C and 3°C throughout the year at all elevations in the Salt, Verde and Rio Grande basins. Additionally, precipitation is not projected to change in any substantial way for the HadCM3 model, while the MPI is projecting a future with slightly less precipitation on average.

When these dynamically downscaled, bias corrected climate variables from both GCMs are

used to force the VIC hydrologic model, statistically significant decreases in streamflow were observed for all three basins. On average, the HadCM3 model projects a 19% decrease in streamflow across the three subbasins, while the MPI projects a 35% decrease. Thus, even with the HadCM3 model, which is projecting approximately the same amount of future precipitation, substantial decreases in streamflow are expected. This is due to significant reductions in SWE and baseflow across the basins in the future.

To extend this research, additional GCM models can be downscaled with more climate change scenarios. This can shed light on the full distribution of projected future streamflow amounts, and provide insight as to whether these initial projections are near the median or the extremes of expected water resources under a changing climate. Also, the RCMs could be run at a higher resolution (<32km), thereby better resolving certain physical processes (e.g., convective precipitation).

Past studies have shown that climate change will alter the timing of streamflow due to warmer temperatures and earlier snowmelt [*Barnett et al.*, 2005; *Cayan*, 2000; *Stewart et al.*, 2004]. Given the importance of an already stressed resource in the Southwest, it is imperative to understand how the total volume of water may also change. With an initial set of models, using the A1B climate change scenario, the streamflows of the Southwest appear to be under threat. More studies that expand upon these results using additional model runs will fill in the distribution of possible futures. However, before access to all of those results are obtained, water managers should think about setting contingency plans for a drier Southwest.

References

Acharya, A., T. C. Piechota, and G. Tootle (2012), Quantitative Assessment of climate change impacts on the hydrology of the North Platte river watershed, Wyoming, *J. Hydrol. Eng., 17,* 1071-1083.

Allen, M. R., and W. J. Ingram (2002), Constraints on future changes in climate and the hydrologic cycle, *Nature, 419,* 224-232.

Barnett, T. P., J. C. Adam, and D. P. Lettenmaier (2005), Potential impacts of a warming climate on

water availability in snow-dominated regions, *Nature, 438,* 303-309.

Castro, C. L., R. A. Pielke Sr., and G. Leoncini (2005), Dynamic downscaling: assessment of value retained and added using the regional atmospheric modeling system (RAMS), *J. Geophys. Res., 110,* D05108, doi:1029/2004JD004721.

Cayan, D. R., S. A. Kammerdiener, M. D. Dettinger, J. M. Caprio, and D. H. Peterson (2001), Changes in the onset of spring in the western United States, *BAMS*, 82 (3), 399-415.

Christensen, N. S., A. W. Wood, N. Voisin, D. P. Lettenmaier, and R. N. Palmer (2004), The effects of climate change on the hydrology and water resources of the Colorado river basin, *Climate Change, 62,* 337-363.

Dominguez, F., E. Rivera, D. P. Lettenmaier, and C. L. Castro (2012), United States under a warmer climate as simulated by regional climate models, *Geophys. Res. Lett., 39,* L05803, doi:10.1029/2011GL050762.

Frich, P., L. V. Alexander, P. Della-Marta, B. Gleason, M. Haylock, A. M. G. Klein Tank, and T. Peterson (2002), Observed coherent changes in climatic extremes during the second half of the twentieth century, *Clim. Res., 19,* 193-212.

Gao, Y., J. A. Vano, C. Zhu, and D. P. Lettenmaier (2011), Evaluating climate change over the Colorado river basin using regional climate models, *J. Geophys. Res., 116,* D13104, doi:10.1029/2010JD015278.

Gupta, H. V., H. Kling, K. K. Yilmaz, and G. F. Martinez (2009), Decomposition of the mean squared error and NSE performance criteria: implications for improving hydrological modelling, *J. Hydrol., 377,* 80-91.

Hamlet, A. F., and D. P. Lettenmaier (1999), Effects of climate change on hydrology and water resources in the Columbia river basin, *J. Am. Water Resour. As., 35 (6),* 1597-1623.

Held, I. M., and B. J. Soden (2006), Robust responses of the hydrological cycle to global warming, *J. Climate, 19,* 5686-5699.

Karl, T. R., K. E. Trenberth (2003), Modern global climate change, *Science, 302,* 1719-1723.

Maurer, E. P., A. W. Wood, J. C. Adam, D. P. Lettenmaier, and B. Nijssen (2002), A long-term hydrologically based dataset of land surface fluxes and states for the conterminous United States, *J. Climate, 15,* 3237-3251.

Maurer, E. P., and H. G. Hidalgo (2008), Utility of daily vs. monthly large-scale climate data: an intercomparison of two statistical downscaling methods, *Hydrol. Earth Syst. Sci., 12*, 551-563.

Milly, P. C. D., K. A. Dunne, and A. V. Vecchia (2005), Global pattern of trends in streamflow and water availability in a changing climate, *Nature, 438 (17),* 347-350.

Milly, P. C. D., J. Betancourt, M. Falkenmark, R. M. Hirsch, Z. W. Kundzewicz, D. P. Lettenmaier, and R. J. Stouffer (2008), Stationarity is dead: whither water management?, *Science, 319,* 573-574.

Murphy, J. (2000), Predictions of climate change over Europe using statistical and dynamical downscaling techniques, *Int. J. of Climatol., 20*, 489-501.

Stewart, I. T., D. R. Cayan, and M. D. Dettinger (2004), Changes in snowmelt runoff timing in western north america under a 'business as usual' climate change scenario, *Climate Change, 62*, 217-232.

Stewart, I. T., D. R. Cayan, M. D. Dettinger (2005), Changes toward earlier streamflow timing across western north America, *J. Climate, 18*, 1136-1155.

Sungwook, W., F. Dominguez, M. Durcik, J. Valdes, H. F. Diaz, and C. L. Castro (2012), Climate change projection of snowfall in the Colorado river basin using dynamical downscaling, *Water Resour. Res., 48*, W05504, doi:10.1029/2011WR010674.

Teutschbein, C. and J. Seibert, Bias correction of regional climate model simulations for hydrological climate-change impact studies: review and evaluation of different methods, *J. Hydrol., 456-457*, 12-29.

Vano, J. A., T. Das, and D. P. Lettenmaier (2012), Hydrologic sensitivities of colorado river runoff to changes in precipitation and temperature, *J. Hydrometeorol., 13*, 932-949.

Von Storch, H., E. Zorita, and U. Cubasch (1993), Downscaling of global climate change estimates to regional scales: an application to Iberian rainfall in wintertime, *J. Climate, 6*, 1161-1171.

Wilby, R. L., T. M. L. Wigley, D. Conway, P. D. Jones, B. C. Hewitson, J. Main, and D. S. Wilks

(1998), Statistical downscaling of general circulation model output: a comparison of methods, *Water Resour. Res., 34 (11)*, 2995-3008.

Wood, A. W., L.R. Leung, V. Sridhar, and D. P. Lettenmaier (2004), Hydrologic implications of dynamical and statistical approaches to downscaling climate model outputs, *Climate Change*, *62*, 189-216.

Tables

	Precipitation (mm)		Max Temp (°C)		Min Temp (°C)		Wind (m/s)	
	Raw	BC	Raw	BC	Raw	BC	Raw	BC
Salt-HadCM3	1.95	.38	2.99	.27	4.09	.27	2.40	.12
Salt-MPI	3.60	.36	4.37	.27	4.16	.28	3.03	.11
Verde-HadCM3	1.89	.35	3.46	.28	3.90	.28	2.56	.09
Verde-MPI	3.19	.31	4.85	.27	3.52	.28	3.27	.07
Rio-HadCM3	2.02	.48	2.76	.32	6.28	.27	2.12	.14
Rio-MPI	1.84	.41	4.03	.41	5.54	.28	2.82	.12

Table 1: The Mean Absolute Error (MAE) values of the raw climate variables and after they were bias corrected (BC).

Figures

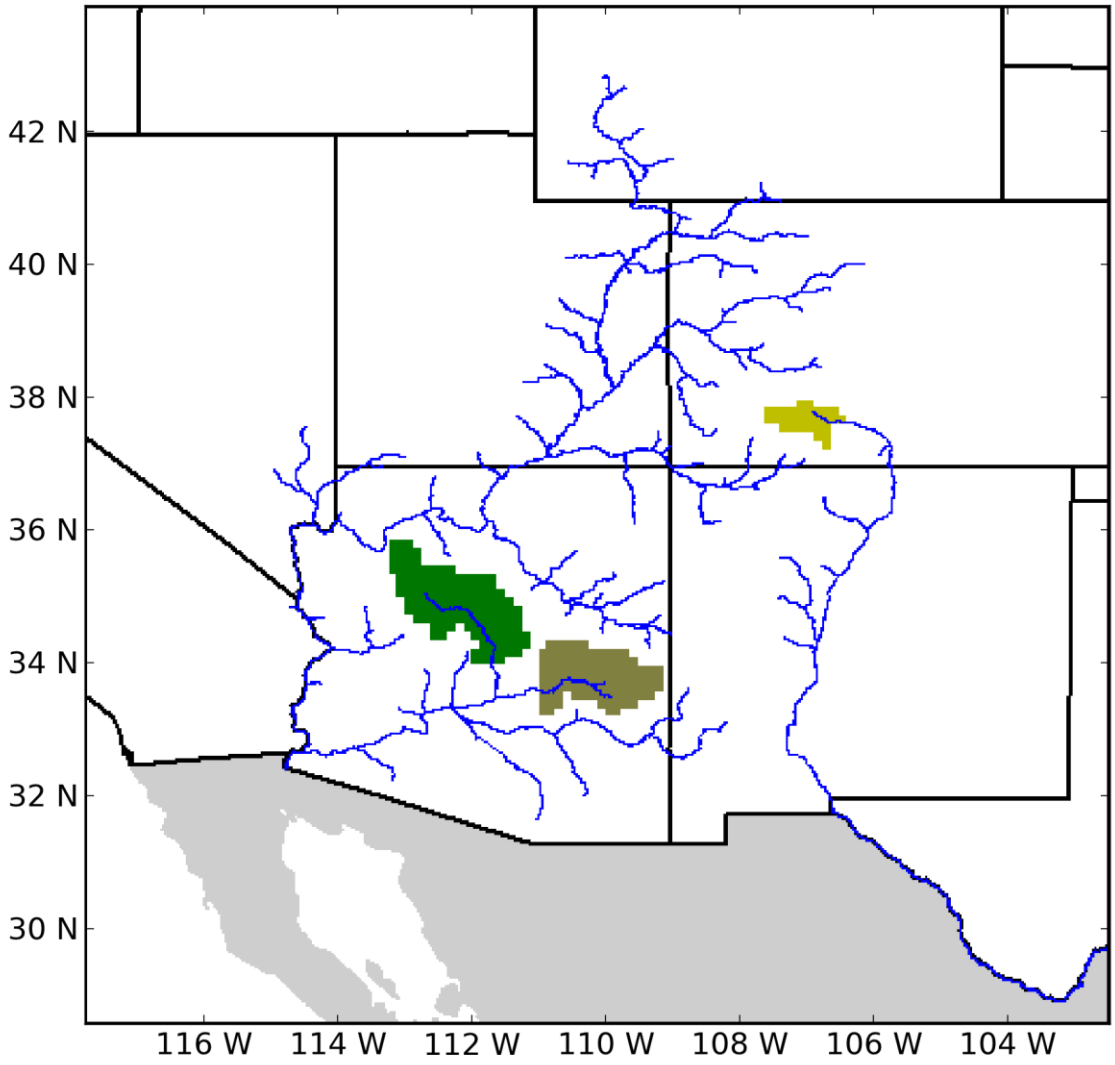

Figure 1: The three basins used are the Verde (green), Salt (tan), and the Rio Grande headwaters (gold).

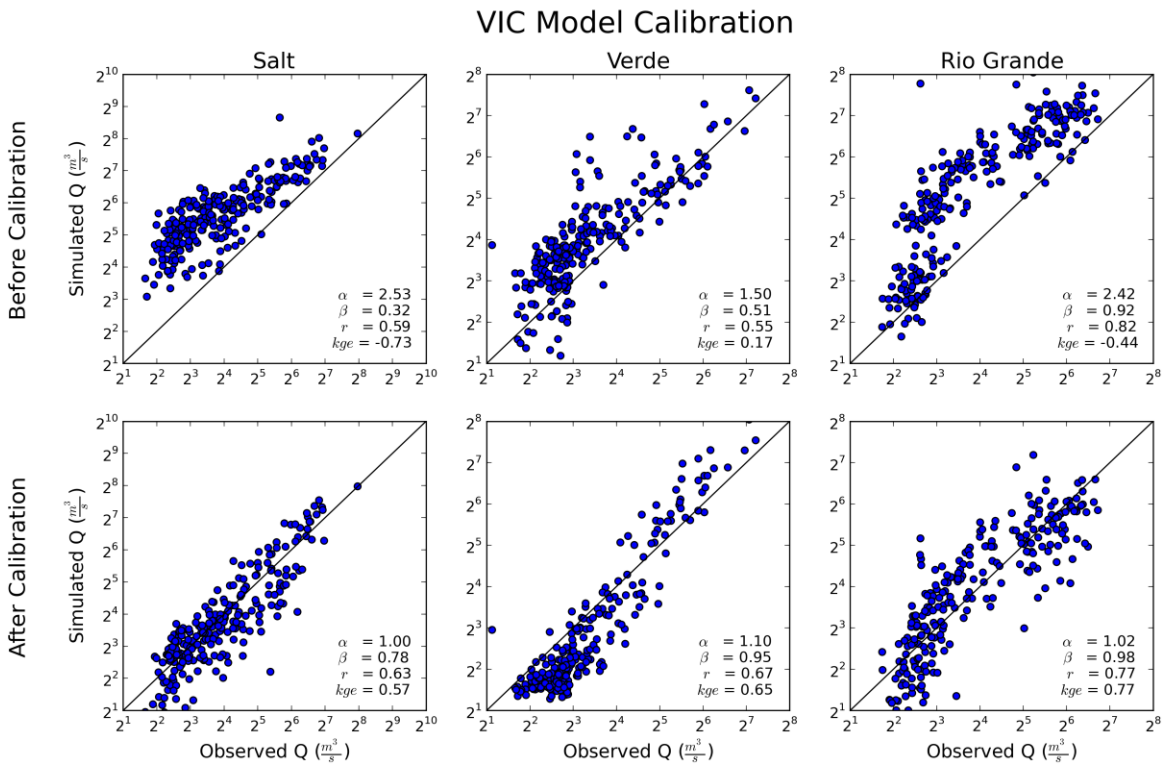

Figure 2: Observed versus simulated streamflows before and after calibration. All components of the KGE as well as the value itself are inset. Substantial reductions in the bias can be seen for the Salt and Rio Grande basins.

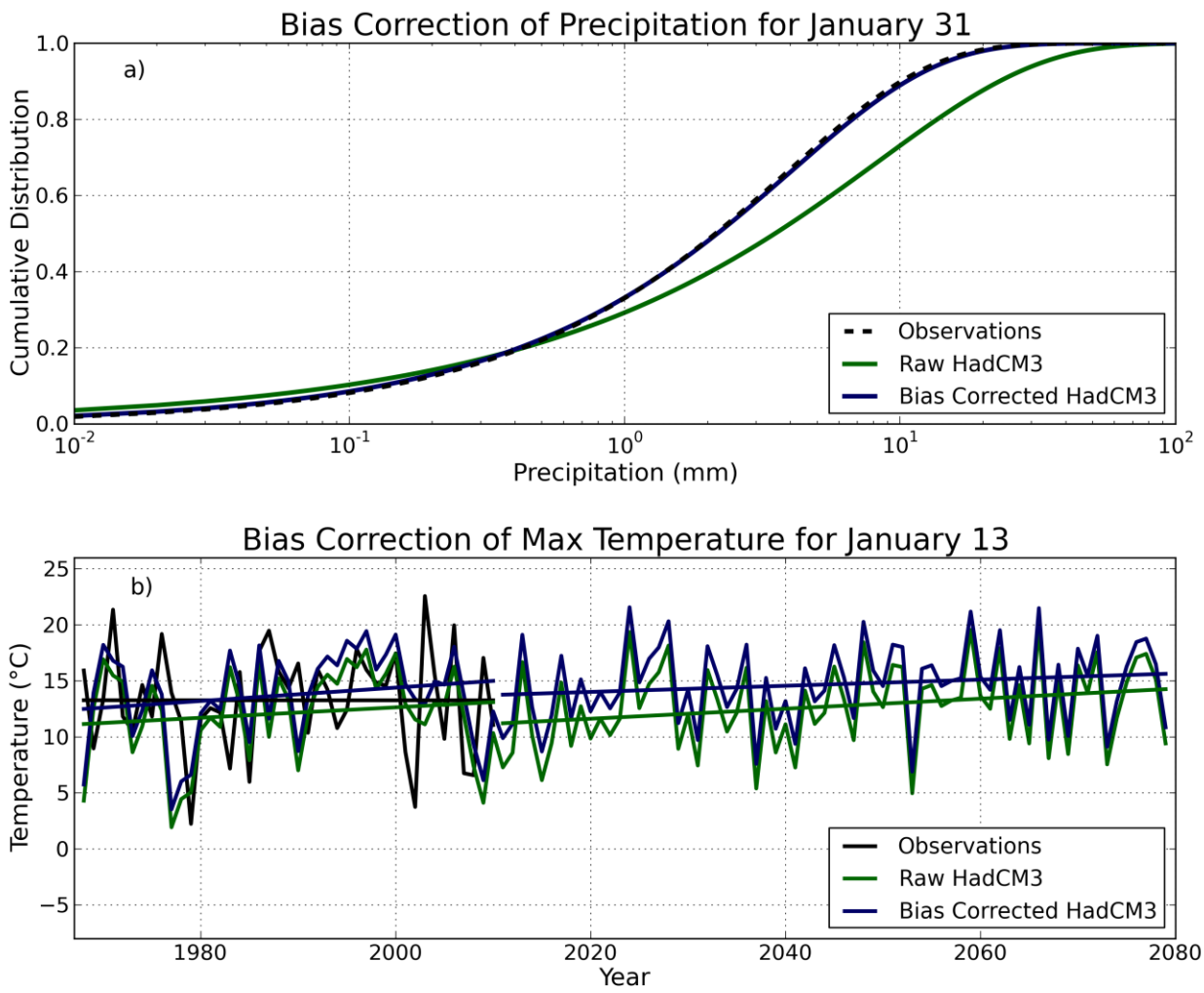

Figure 3: Subplot a) shows the shifting of the HadCM3 precipitation CDF, due to bias correction, for the example date of January 31st. Fitted observations are the dashed black line, the raw fitted data is the green line, and the bias corrected fit is the blue line. Subplot b) shows the time series of bias corrected max temperature for all January 13th days. The means and variances are shifted to match observations, while the trends are preserved.

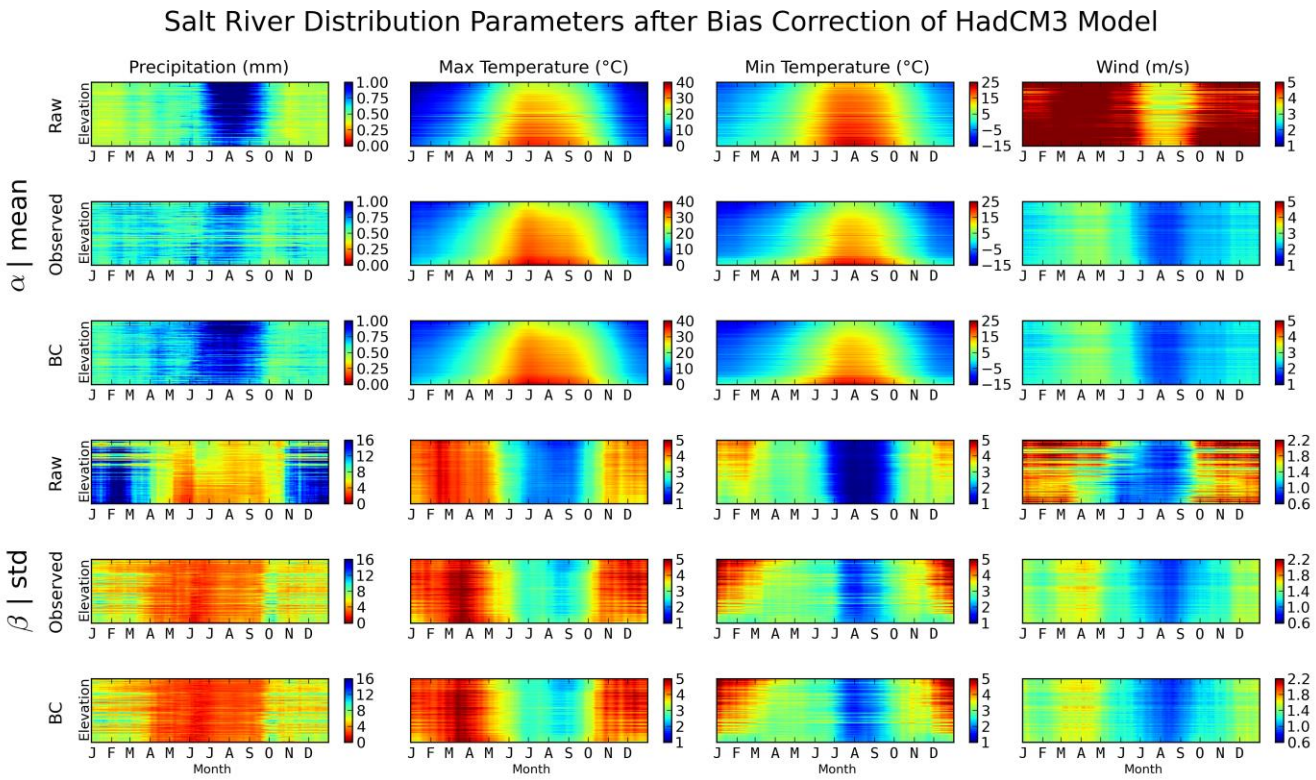

Figure 4: The raw distribution parameters α and mean correspond to the upper three rows of subplots, while β and standard deviation correspond to the bottom three rows. The first and fourth rows show the raw distribution parameters. The second and fifth rows show the observed parameters. The third and sixth rows show the bias corrected parameters. The x-axis are the days of the year with the months shown. The y-axis is sorted elevation for the Salt river, with the highest elevation on top. Ideally, if the bias corrected variable had very similar distributions to observations, rows two and three should like identical and similarly for five and six.

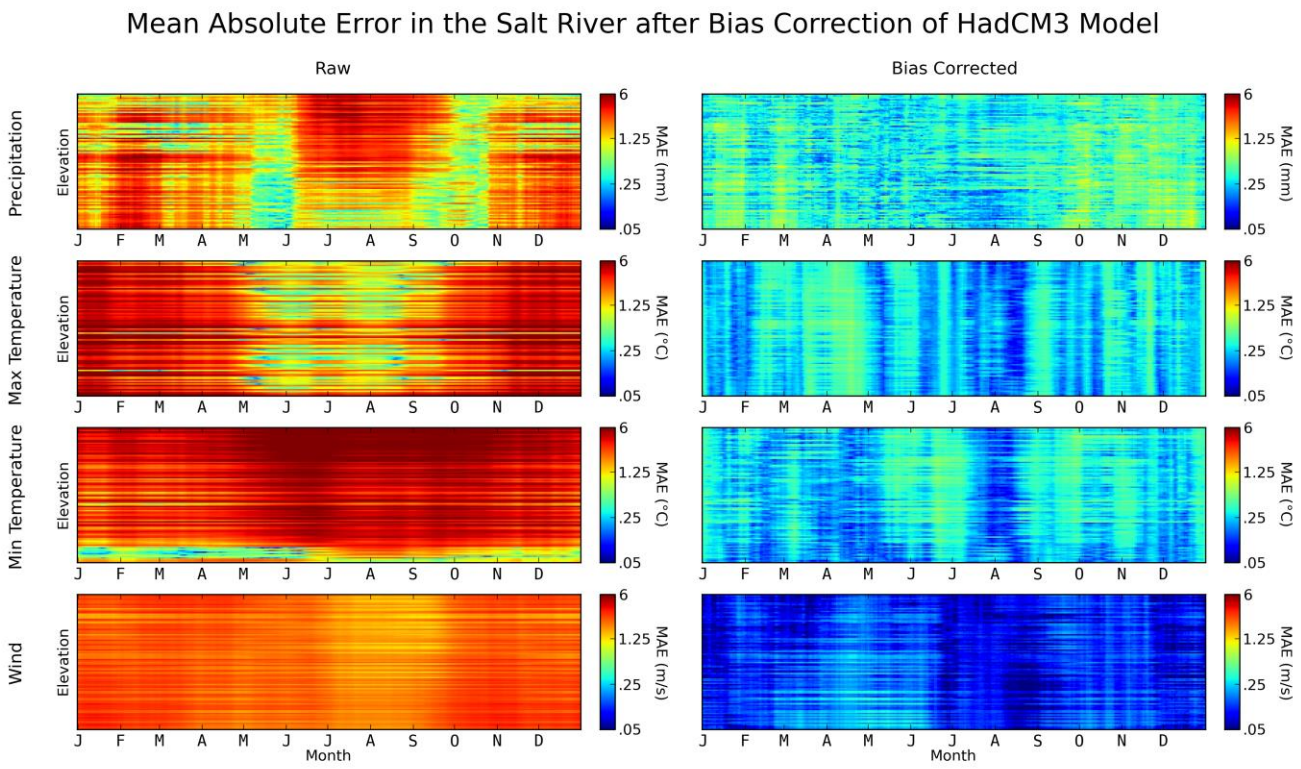

Figure 5: Example of the Mean Absolute Errors for the raw climate variables and after bias correction.

The x and y-axes are the same as figure 4. The colorbars are logarithmic.

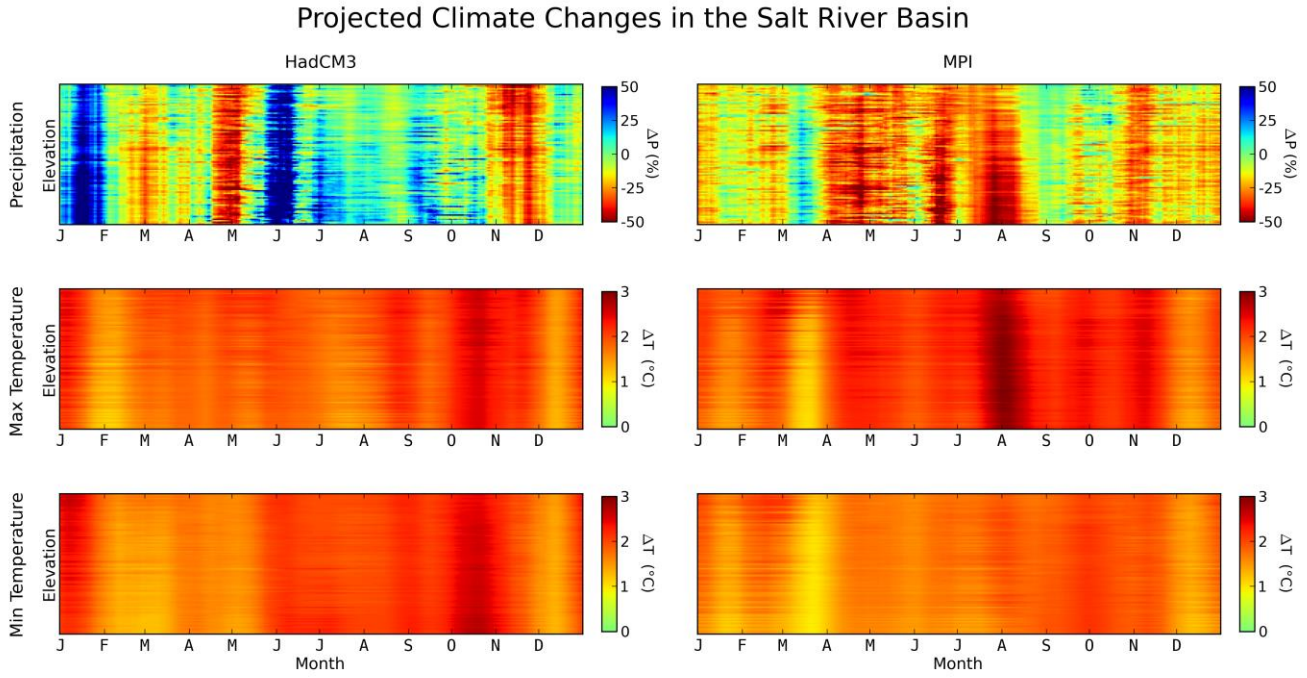

Figure 6: Projected climate changes in the Salt river basin for both the HadCM3 and MPI models. The x and y axes are same as Figures 4 and 5. The colorbars for precipitation show the percentage change in projected future values with respect to past values. The temperature colorbars show the difference between projected future values with respect to past values.

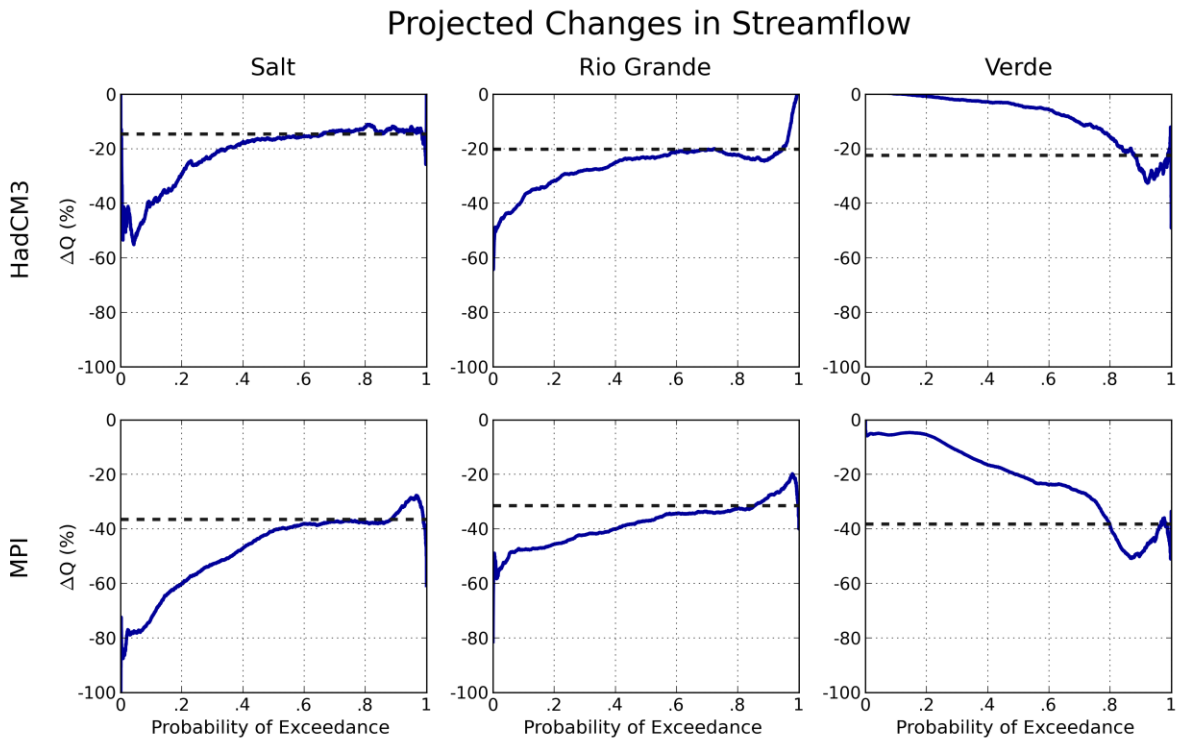

Figure 7: Projected average streamflow changes, for each probability of exceedance, in reference to the modeled data prior to the year 2011. Both models are projecting greater decreases at high flows than at low flows for the Salt and Rio Grande, while the opposite is true for the Verde.

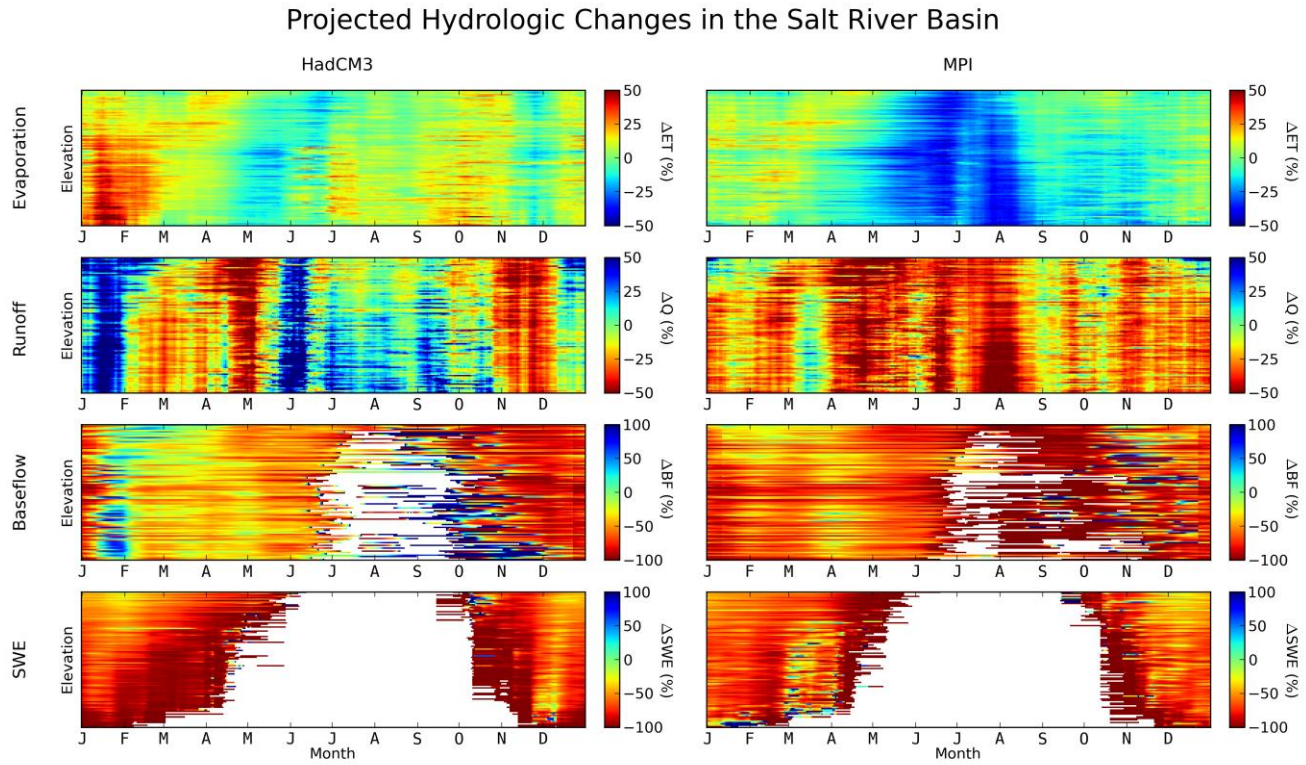

Figure 8: Projected hydrologic changes in the Salt river basin for both the HadCM3 and MPI models. These variables were obtained from the VIC model. The colorbars show the percentage changes of the projected future values with respect to the past values. The variables are evaporation, runoff, baseflow and snow water equivalent (SWE), respectively.